Application of Finite-Integral Technique to Electromagnetic Scattering by Two-Dimensional Cavity-Backed Aperture in a Ground Plane

Sadasiva M. Rao, *Senior Member, IEEE*, Griffin K. Gothard, and Donald R. Wilton, *Fellow, IEEE*

***Abstract*— In this work, we analyze the electromagnetic scattering by a cavity-backed two-dimensional (2-D) aperture in a ground plane illuminated by either a TE or TM plane wave. The analysis is based on the well-known generalized network formulation. To obtain the admittance matrix of the cavity, the cavity is modeled by triangular cylinders. Also, in order to specify inhomogeneous materials, a separate ϵ and μ may be assigned to each cylinder. Further, the cavity is analyzed applying the finite-integral technique (FIT), which results in spurious-free solution. Finally, numerical examples are presented to illustrate the applicability of the method.**

***Index Terms*—Electromagnetic scattering, numerical analysis.**

I. Introduction

THE problem of electromagnetic field penetration into an arbitrarily shaped cavity backing an aperture in a ground plane has received considerable attention because of the applications in aerospace and communications industry. Traditionally, these type of problems have been analyzed using the mode matching [1] and the modal solutions via method of moments [2]. Unfortunately, these methods are applicable to rectangular cavities only which is quite restrictive. Recently, however, the finite-element (FE) method received increased attention for the the field penetration problem because: 1) the FE approach generates a highly sparse system matrix and 2) modeling inhomogeneous regions and arbitrary geometries is straightforward. In fact, the two-dimensional (2-D) cavity-backed aperture problem using FE method was already solved [3], [4]. However, the main disadvantage of the FE method is the presence of spurious solutions, which sometimes leads to inaccurate and oscillatory solutions.

In this work, we present an alternate approach to solve the electromagnetic field penetration into a cavity backing an infinitely long slot. The approach is termed as finite-integral technique (FIT) [5]–[7]. The FIT uses the integral form of Maxwell's equations applied to a discrete conformal grid. The cavity volume is subdivided into triangular cylinders and constitutive material parameters are assigned to each cylinder, thus facilitating the specification of an inhomogeneous region. Further, the unknown vector electric and magnetic fields are approximated by specially designed basis functions with unknown coefficients. These basis functions let us satisfy all the required continuity conditions of the electric and magnetic fields at every material boundary. Some of the major advantages of the FIT approach may be listed as follows.

1) The present approach requires minimal computer storage, thereby enabling us to solve electrically large problems.
2) Modeling of various materials is very simple.
3) User-defined basis function provides a better control on the algorithm and enables us to satisfy all the boundary and continuity conditions accurately.
4) The usage of the integral form of Maxwell's equations provide a smoothing effect on the solution obtained.
5) Spurious solutions are not observed in the present formulation; the absence of spurious solutions may be due to the usage of specially developed basis functions.

The paper is organized as follows. In the next section, a detailed mathematical formulation of the FIT scheme for the TE case is provided. Here, we describe specially designed basis functions to approximate the unknown electric and magnetic fields. Further, we provide the detailed mathematical description of the application of the FIT to the problem under consideration. In Section III, we discuss the application of FIT to the TM problem. Numerical examples are presented in Section IV to demonstrate the validity of the FIT approach. Finally, some important conclusions are drawn from this study are presented in Section V.

II. Transverse Electric Case

Consider a cavity-backed 2-D slit (as shown in Fig. 1) illuminated by an incident plane wave given by

$$\mathbf{H}^i = H_0 e^{jk(x\cos\phi + y\sin\phi)}\mathbf{a}_z \tag{1}$$

where $\mathbf{H}_i$ is the incident magnetic field plane wave, k is the wavenumber, and ϕ is the angle of arrival of the plane wave. By the TE assumption, the incident as well as the scattered magnetic field is in the z direction and the electric field is in the xy plane.

By using the generalized network formulation [8], the problem at hand may be separated into three subproblems, viz.: 1) radiation problem; 2) short-circuit problem; and 3)

Manuscript received March 11, 1997; revised December 12, 1997. This work was supported by Texas Instruments Inc., McKinney, TX.

S. M. Rao is with the Department of Electrical Engineering, Auburn University, Auburn, AL 36849 USA.

G. K. Gothard is with the Harris Corporation, Melbourne, FL 32902 USA.

D. R. Wilton is with the Department of Electrical and Computer Engineering, University of Houston, Houston, TX 77204 USA.

Publisher Item Identifier S 0018-926X(98)03400-0.

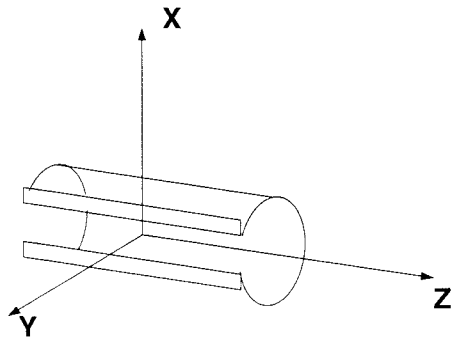

Fig. 1. Cavity-backed slit.

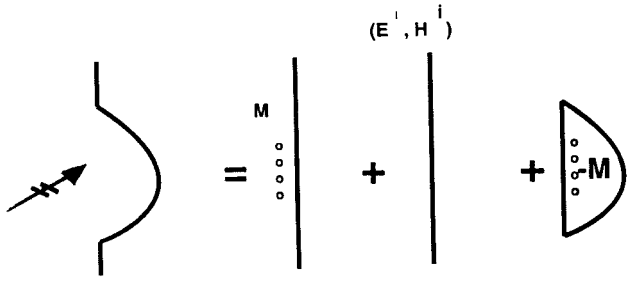

Fig. 2. Equivalent problems.

cavity problem as shown in Fig. 2. For the radiation and cavity problems, an equivalent magnetic surface current $\mathbf{M} = M(x)\mathbf{a}_z$ and it's negative are attached on the exterior and the interior side of the closed aperture. Dividing the aperture region into N equal subdomains and following the procedures described in [3], we have

$$[[Y^R] + [Y^C]][V] = [I]. \tag{2}$$

The evaluation of $[Y^R]$ and $[I]$ is straight forward and well presented in [3]. The admittance matrix $[Y^C]$ is the admittance of the cavity. In this work, the matrix elements of $[Y^C]$ are obtained by applying the FIT method as discussed in the following subsection.

A. Evaluation of $[Y^C]$ Using FIT Formulation

The FIT directly applies the Maxwell equations in integral form to a discrete grid. Maxwell's equations in the integral form are given by

$$\int_s (\nabla \times \mathbf{E}) \cdot \mathbf{a}_n \, ds = -\jmath\omega \int_s \mu \mathbf{H} \cdot \mathbf{a}_n \, ds + \int_s \mathbf{M} \cdot \mathbf{a}_n \, ds \tag{3}$$

$$\int_s (\nabla \times \mathbf{H}) \cdot \mathbf{a}_n \, ds = \jmath\omega \int_s \epsilon \mathbf{E} \cdot \mathbf{a}_n \, ds \tag{4}$$

where $\mathbf{H}$ is the magnetic field, $\mathbf{E}$ is the electric field, ϵ is the permittivity, and μ is the permeability of the region bounded by the surface S. Also, $\mathbf{M} = M_0 \delta(\boldsymbol{\rho} - \boldsymbol{\rho}')\mathbf{a}_z$ is the magnetic current exciting the cavity. Further, for the 2-D TE case, the magnetic field is along the z direction and the electric field is confined to the transverse plane (xy plane).

First, consider (3). Applying Stoke's theorem to an arbitrary closed surface in the xy plane (as shown in Fig. 3) and

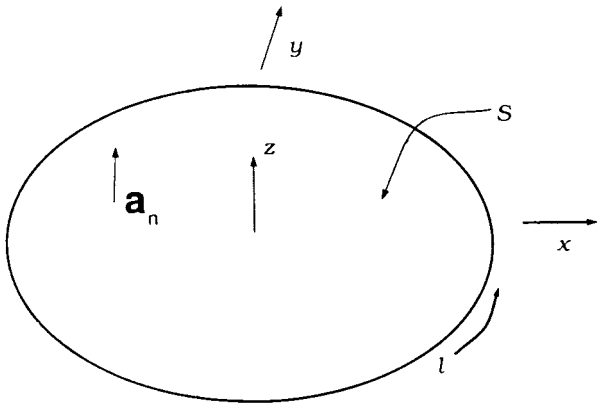

Fig. 3. The area of integration S with the normal vector $\mathbf{n}$ in the z direction.

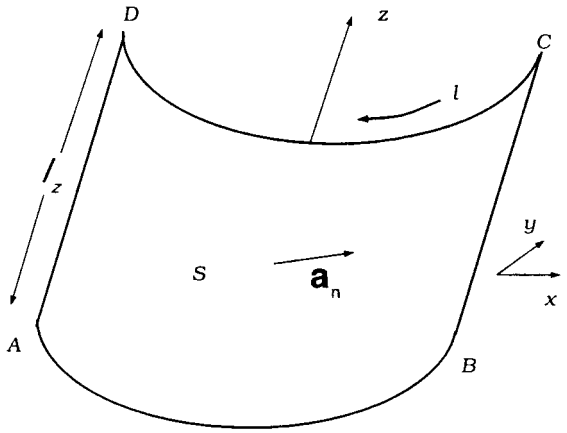

Fig. 4. The area of integration S with the normal vector $\mathbf{n}$ in the xy (transverse) plane. The value l_z is the length of S along the z direction.

utilizing the fact that $\mathbf{H} = H_z \mathbf{a}_z$ yields

$$\oint_l \mathbf{E}_t \cdot \mathbf{dl} = -\jmath\omega \int_s \mu H_z \, ds + M_0 \tag{5}$$

where l is the closed path about the surface S, $\mathbf{E}_t$ is the TE field, and H_z is the magnetic field in the z direction.

Next, consider (4). For this equation, define the surface S such that the normal vector $\mathbf{a}_n$ lies in the xy plane, as shown in Fig. 4. Again, applying Stoke's theorem to (4) yields

$$\oint_l \mathbf{H} \cdot \mathbf{dl} = \jmath\omega \int_s \epsilon \mathbf{E} \cdot \mathbf{a}_n \, ds. \tag{6}$$

In (6), the path of integration is along the contour of S as shown in Fig. 4. This path lies along segments AB, BC, CD, and DA. Also, note that along paths AB and CD, $\mathbf{H} \cdot \mathbf{dl} = 0$, since $\mathbf{dl}$ is perpendicular to z. Thus, we have

$$\oint_l \mathbf{H} \cdot \mathbf{dl} = \left(H_z^{AD} - H_z^{BC}\right) l_z \tag{7}$$

where H_z^{AD} and H_z^{BC} are the magnetic fields at AD and BC, respectively, and l_z is the length of S along the z direction. Further, noting that all field quantities are invariant with z, we have

$$\jmath\omega \int_s \epsilon \mathbf{E} \cdot \mathbf{a}_n \, ds = \jmath\omega \int_z \int_l \epsilon \mathbf{E}_t \cdot \mathbf{a}_n \, dl \, dz = \jmath\omega l_z \int_l \epsilon \mathbf{E}_t \cdot \mathbf{a}_n \, dl. \tag{8}$$

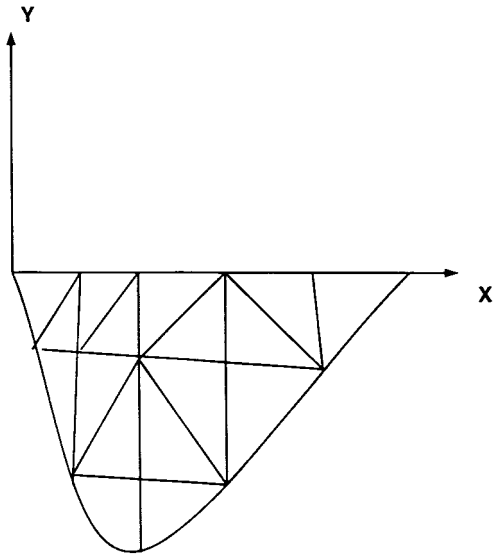

Fig. 5. A 2-D cavity represented by triangular cylinders.

Finally, using (7) and (8), (4) may be written as

$$H_z^{AD} - H_z^{BC} = \jmath\omega \int_l \epsilon \mathbf{E}_t \cdot \mathbf{a}_n \, dl. \tag{9}$$

B. Description of Basis Functions

In the FIT scheme, the 2-D cavity is approximated by triangular cylinders as shown in Fig. 5. Let N_I, N_J, and N_K represent the number of vertices, faces, and edges, respectively, in the grid scheme. Next, we define two sets of basis functions as follows.

Referring to Fig. 6(a), we define the first set of functions $\Pi_j(\boldsymbol{\rho})$ as

$$\Pi_j(\boldsymbol{\rho}) = \begin{cases} 1.0, & \boldsymbol{\rho} \in T_j \\ 0.0, & \text{otherwise} \end{cases} \tag{10}$$

where T_j represents the region on face j.

Next, referring to Fig. 6(b) we define another set of functions, the rooftop functions developed by Rao *et al.* [9] for each edge as

$$\wedge_k(\boldsymbol{\rho}) = \begin{cases} \wedge_k^{\pm}(\boldsymbol{\rho}), & \boldsymbol{\rho} \in T_k^{\pm} \\ 0.0, & \text{otherwise} \end{cases} \tag{11}$$

where $\wedge_k^+ = \frac{\rho_k^+}{\mathbf{h}_\mathbf{k}^+}$ and h_k^+ is the height of the free vertex in the triangle T_k^+ from edge k. $\wedge_k^-$ is defined identically on triangle T_k^- with variable superscript $(-)$ instead of $+$.

Utilizing these basis functions, the total electric field $\mathbf{E}_t$ and magnetic field H_z existing in the discretized space can be expressed as

$$H_z = \sum_j^{N_J} H_j \Pi_j(\boldsymbol{\rho}) \tag{12}$$

$$\mathbf{E}_t = \sum_k^{N_K} E_k(\wedge_k(\boldsymbol{\rho}) \times \mathbf{a}_z) \tag{13}$$

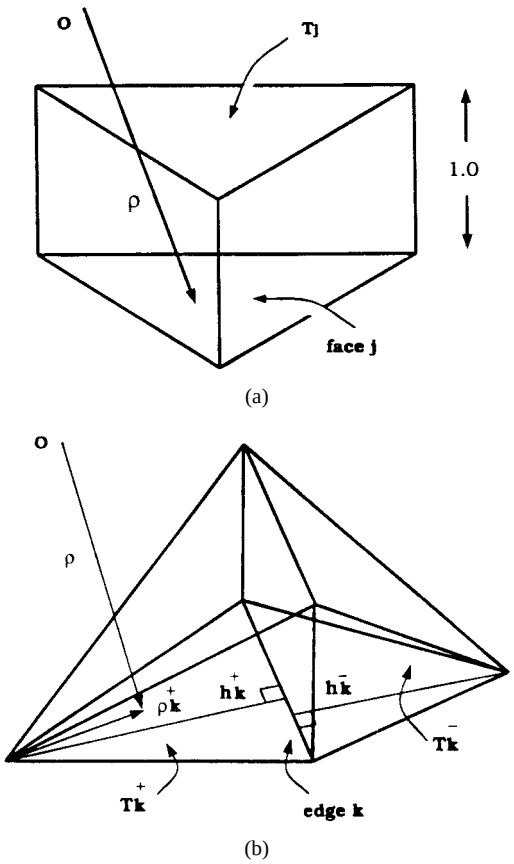

Fig. 6. (a) Pulse function Π_i. (b) $\wedge$ basis function.

where H_j and E_k represent the unknown coefficients to be determined. Note that $\wedge_k(\boldsymbol{\rho}) \times \mathbf{a}_z$ represents a vector directed along the length of the edge k. This representation allows us to enforce the continuity of tangential electric fields at material boundaries.

C. Numerical Analysis

The next step in the FIT procedure is to determine a discrete expression for the integral form of Maxwell's equations, which will be used to generate the FIT global matrix. This is accomplished by using the basis functions as defined in (12) and (13) to provide approximations for the TE and axial magnetic fields in (5) and (9). The resulting simplified equations will be combined to eliminate the TE field unknowns, resulting in a system of equations in terms of the magnetic field unknowns only. This is accomplished as follows by referring to a triangular patch j, as shown in Fig. 7.

Now, consider the left-hand side of (5). The integral is defined over a closed path l, which can be defined around the three edges composing each face j. This yields

$$\oint_l \mathbf{E}_t \cdot \mathbf{dl} = \int_{\text{edge}\#1} \mathbf{E}_t \cdot \mathbf{dl} + \int_{\text{edge}\#2} \mathbf{E}_t \cdot \mathbf{dl} + \int_{\text{edge}\#3} \mathbf{E}_t \cdot \mathbf{dl}. \tag{14}$$

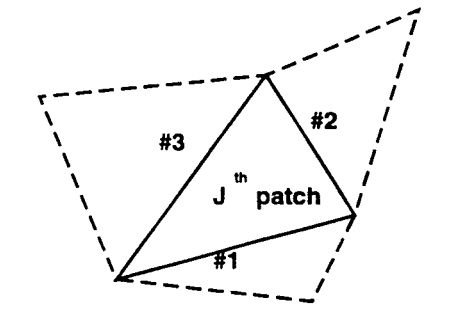

(a)

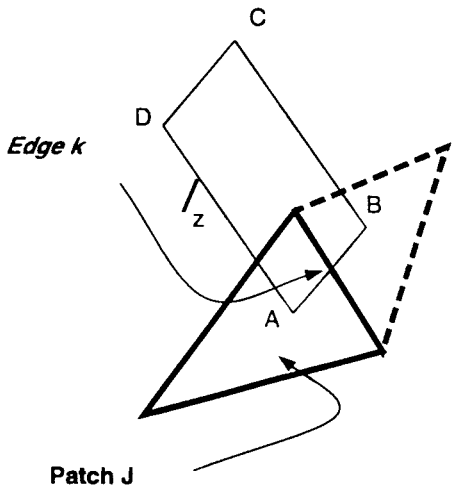

(b)

Fig. 7. A triangular face j with adjacent triangles.

Applying the rooftop function defined in (11) for an individual edge k, $k = 1$, 2, and 3 in (14) yields

$$\int_k \mathbf{E}_t \cdot \mathbf{dl} = E_{jk} \int_k (\wedge_{jk}(\boldsymbol{\rho}) \times \mathbf{a}_z) \cdot \mathbf{dl} = E_{jk} \int_k \wedge_{jk}(\boldsymbol{\rho}) \cdot \mathbf{a}_n \, dl = E_{jk} \sigma_{jk} l_{jk} \tag{15}$$

where $\sigma_{jk} = 1.0$ if $\wedge_{jk}$ and $\mathbf{a}_n$ are in the same direction, otherwise -1.0, and l_{jk} is the length of the edge k. Thus, using (15), we can rewrite (14) as

$$\oint_l \mathbf{E}_t \cdot \mathbf{dl} = \sum_{k=1}^{3} E_{jk} \sigma_{jk} l_{jk}. \tag{16}$$

Next, consider the right-hand side of (5). Substituting the Π_j function defined by (10) for the magnetic field yields for face j

$$-\jmath\omega \int_s \mu H_z \, ds + M_0 = -\jmath\omega\mu_j H_j A_j + M_0 \tag{17}$$

where μ_j is the permeability associated with face j, A_j is the area of face j, and H_j is the unknown magnetic field quantity, defined at the centroid of face j.

Thus, using (16) and (17), (5) may be written as

$$\sum_{k=1}^{3} E_{jk} \sigma_{jk} l_{jk} = -\jmath\omega\mu_j H_j A_j + M_0. \tag{18}$$

Now, let us consider the left-hand side of (9). Referring to Fig. 7 and applying the Π_j function defined in (11) for an edge k, $k = 1$, 2, and 3 yields

$$H_z^{AD} - H_z^{BC} = H_j - H_{jk} \tag{19}$$

where H_j and H_{jk} are the unknown magnetic field quantities at the centroids of the triangles connected to edge k.

Last, consider the right-hand side of (9). Applying the rooftop function defined in (11), we have

$$\begin{aligned} &\jmath\omega \int_k \epsilon \mathbf{E}_t \cdot \mathbf{a}_n \, dl \\ &= \jmath\omega E_{jk} \int_k \epsilon (\wedge_k(\boldsymbol{\rho}) \times \mathbf{a}_z) \cdot \mathbf{a}_n \, dl \\ &= \jmath\omega E_{jk} \left[\int_k \epsilon_j \wedge_k(\boldsymbol{\rho}) \cdot \mathbf{dl} + \int_k \epsilon_{jk} \wedge_{jk}(\boldsymbol{\rho}) \cdot \mathbf{dl} \right] \\ &= \jmath\omega E_{jk} \frac{5 l_{jk}}{36} \left[\frac{\epsilon_j m_j}{A_j} + \frac{\epsilon_{jk} m_{jk}}{A_{jk}} \right] \\ &= \jmath\omega E_{jk} \xi_{jk} \end{aligned} \tag{20}$$

where m_j and m_{jk} are the median lengths from the opposite vertex to the edge k and A_j and A_{jk} are the areas of the triangles connected to edge k.

Thus, using (19) and (20), we can write (9) as

$$E_{jk} = \frac{1}{\jmath\omega\xi_{jk}} [H_j - H_{jk}]. \tag{21}$$

Finally, substituting (21) into (18), we have for jth patch

$$\sum_{k=1}^{3} [H_{jk} - H_j] \frac{\sigma_{jk} l_{jk}}{\xi_{jk}} + \omega^2 \mu_j A_j H_j = -\jmath\omega M_0 \tag{22}$$

where now the unknowns are exclusively in terms of the unknown magnetic field coefficients. Applying (22) for each triangular patch in the grid scheme, a gobal FIT matrix may be generated that is sparse with, at most, four nonzero entries per row. By inverting this matrix and multiplying with the excitation vector, the magnetic field coefficients throughout the cavity region may be calculated. However, we need the magnetic field only at the aperture, which may be obtained as follows.

The elements of Y_{pq}^C are obtained by placing a unit magnetic current source at x_q, $q = 1$, 2, $\cdots$, N, solving (22), and obtaining the corresponding magnetic field at x_p, $p = 1$, 2, $\cdots$, N. This, in effect, implies the evaluation of pqth element of the inverted FIT matrix.

A close examination of (22) reveals that it is, in fact, the finite-difference equation for the triangular grid. Also, it is very easy to derive the traditional finite-difference equation applied to a square grid by following the numerical procedure narrated in this section.

Finally, we mention here that although not attempted in the present work, the frontal solution employed in [3] can also be employed in the FIT scheme.

III. Transverse Magnetic Case

Consider again the cavity-backed 2-D slit shown in Fig. 1, illuminated by a TM incident plane wave given by

$$\mathbf{E}^i = E_0 e^{j\,k(x\cos\phi + y\sin\phi)}\mathbf{a}_z. \tag{23}$$

By using the generalized network formulation [8], again, the problem at hand may be separated into three subproblems, viz.: 1) radiation problem; 2) short-circuit problem; and 3) cavity problem as shown in Fig. 2. For the radiation and cavity problems, an equivalent magnetic surface current $\mathbf{M} = M(x)\mathbf{a}_x$ and its negative are attached on the exterior and the interior side of the closed aperture, respectively. Further, these problems are coupled and may be described by the following equation given by

$$[[Y^R] + [Y^C]][V] = [I]. \tag{24}$$

The evaluation of $[Y^R]$ and $[I]$ is straightforward and well presented in [4]. The admittance matrix $[Y^C]$ is the admittance of the cavity. In the following subsection, we present the evaluation of matrix elements of $[Y^C]$ by applying the FIT method.

A. Evaluation of $[Y^C]$ Using FIT Formulation

First, consider (4). Applying the Stokes theorem to an arbitrary closed surface in the xy plane (as shown in Fig. 3) and utilizing the fact that $\mathbf{E} = E_z\mathbf{a}_z$ yields

$$\oint_l \frac{\mathbf{B}_t}{\mu}\cdot\mathbf{dl} = \jmath\omega\int_s \epsilon E_z\,ds \tag{25}$$

where l is the closed path about the surface S, $\mathbf{B}_t$ is the TM flux density and E_z is the electric field in the z direction.

Next, consider (3). Note that for the TM case, $\mathbf{M} = M_0\delta(\boldsymbol{\rho}-\boldsymbol{\rho}')\mathbf{a}_x$, i.e., along the transverse plane to the axis of the slot. For this equation, define the surface as shown in Fig. 4 and apply the Stokes theorem to obtain

$$\oint_l \mathbf{E}\cdot\mathbf{dl} = -\jmath\omega\int_s \mathbf{B}\cdot\mathbf{a}_n\,ds + \int_s \mathbf{M}\cdot\mathbf{a}_n\,ds. \tag{26}$$

In (26), the path of integration is along the contour of S, as shown in Fig. 4. This path lies along the segments AB, BC, CD, and DA. Note that along paths AB and CD, $\mathbf{E}\cdot\mathbf{dl} = 0$ since $\mathbf{dl}$ is perpendicular to z. Thus, we have

$$\oint_l \mathbf{E}\cdot\mathbf{dl} = \left(E_z^{AD} - E_z^{BC}\right)l_z \tag{27}$$

where E_z^{AD} and E_z^{BC} are the electric fields at AD and BC, respectively, and l_z is the length of S along the z direction. Further, noting that all field quantities are invariant with z we have

$$\begin{aligned}-\jmath\omega\int_s \mathbf{B}\cdot\mathbf{a}_n\,ds &= -\jmath\omega\int_z\int_l \mathbf{B}_t\cdot\mathbf{a}_n\,dl\,dz\\ &= -\jmath\omega l_z\int_l \mathbf{B}_t\cdot\mathbf{a}_n\,dl\end{aligned} \tag{28}$$

and

$$\int_s \mathbf{M}\cdot\mathbf{a}_n\,ds = M_0 l_z\int_l \delta(\boldsymbol{\rho}-\boldsymbol{\rho}')\mathbf{a}_x\cdot\mathbf{a}_n\,dl. \tag{29}$$

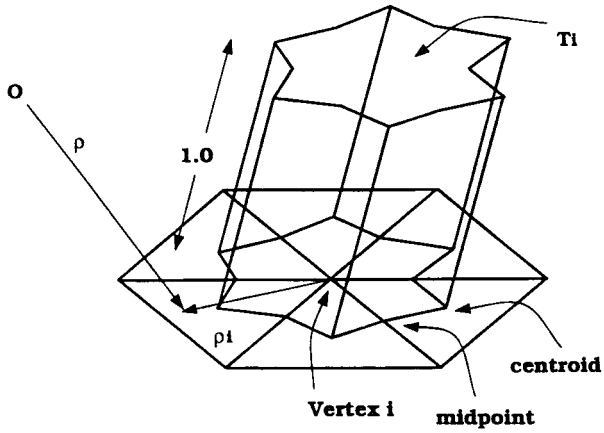

Fig. 8. Pulse function Π_i.

Thus, using (27)–(29), (26) may be written as

$$\begin{aligned}&E_z^{AD} - E_z^{BC}\\ &\quad= -\jmath\omega\int_l \mathbf{B}_t\cdot\mathbf{a}_n\,dl + M_0 l_z\int_l \delta(\boldsymbol{\rho}-\boldsymbol{\rho}')\mathbf{a}_x\cdot\mathbf{a}_n\,dl.\end{aligned} \tag{30}$$

B. Description of Basis Functions

The next step in the numerical scheme is to approximate the 2-D cavity by triangular cylinders, as shown in Fig. 5. Let N_I, N_J, and N_K represent the number of vertices, triangular faces, and edges, respectively, in the grid scheme. Also, let N_B represent the number of vertices on the cavity walls. Next, we look at the basis functions.

Referring to Fig. 8, we define the a set of functions termed as the pulse functions $\Pi_i(\boldsymbol{\rho})$ as

$$\Pi_i(\boldsymbol{\rho}) = \begin{cases}1.0 & \boldsymbol{\rho}\in T_i\\ 0.0 & \text{otherwise}\end{cases} \tag{31}$$

where T_i represents the region obtained by assembling all the triangles connected to vertex i and joining the centroids of each triangle to the midpoints of each edge connected to vertex i. Note that each T_i represents a closed contour, provided vertex i is not a boundary vertex.

Next, the total electric field E_z and magnetic flux density $\mathbf{B}_t$ existing in the discretized space can be expressed as

$$E_z = \sum_i^{N_I} E_i\Pi_i(\boldsymbol{\rho}) \tag{32}$$

$$\mathbf{B}_t = \sum_k^{N_K} B_k\wedge_k(\boldsymbol{\rho}) \tag{33}$$

where E_i and B_k represent the unknown coefficients to be determined. Note that $\wedge_k(\boldsymbol{\rho})$, defined in (11), has a continuous normal component along each edge. This property is important in enforcing continuity of the magnetic flux density at material boundaries.

C. Numerical Analysis

Consider an interior vertex i, as shown in Fig. 9. Vertices $i^i = 1, 2, \cdots, I^i$ connect the edges $k^i = 1, 2, \cdots, K^i$ to the vertex i, and $j^i = 1, 2, \cdots, J^i$ represent the triangles

connected to vertex i. Using this notation, we will derive the finite-integral discretized form of (25) and (30).

Consider the left-hand side of (25). Substituting the rooftop function defined in (11) we have

$$\begin{aligned}\oint_l \frac{\mathbf{B}_t}{\mu}\cdot\mathbf{dl} &= \sum_{k^i=1}^{K^i}\frac{B_{k^i}}{\mu}\oint_{l_{k^i}} \wedge_{k^i}(\boldsymbol{\rho})\cdot\mathbf{dl}\\ &= \sum_{k^i=1}^{K^i} B_{k^i}\frac{5l_{k^i}}{36}\left[\frac{m^+_{k^i}}{\mu^+_{k^i}A^+_{k^i}}+\frac{m^-_{k^i}}{\mu^-_{k^i}A^-_{k^i}}\right]\\ &= \sum_{k^i=1}^{K^i} B_{k^i}\nu_{k^i} \end{aligned} \tag{34}$$

where $T^{\pm}_{k^i}$ are the triangles connected to edge k^i, $m^{\pm}_{k^i}$ are the median lengths from the opposite vertex to the edge k^i, and $A^{\pm}_{k^i}$ are the areas of the triangles $T^{\pm}_{k^i}$.

Next, let us look at the right-hand side of (25). Substituting the Π_i basis function defined by (31) for the electric field yields, for any vertex i

$$\begin{aligned}\jmath\omega\int_s \epsilon E_z\,ds &= \jmath\omega\epsilon\int_{\partial T_i} E_i\Pi_i(\boldsymbol{\rho})\,ds\\ &= \jmath\omega E_i\sum_{j^i=1}^{J^i}\epsilon_{j^i}\frac{A_{j^i}}{3}\end{aligned} \tag{35}$$

where ∂T^i is the contour of the $\Pi_i(\boldsymbol{\rho})$ subdomain and ϵ_{j^i} and A_{j^i} are the permittivity and area, respectively, associated with face j^i.

Substituting (34) and (35) into (25) yields

$$\sum_{k^i=1}^{K^i} B_{k^i}\nu_{k^i} = \jmath\omega E_i\sum_{j^i=1}^{J^i}\epsilon_{j^i}\frac{A_{j^i}}{3}. \tag{36}$$

Next, consider left-hand side of (30). Referring to Fig. 9 and applying the II function to a vertex i yields for any edge $k^i = 1, 2, \cdots, K^i$ connected to vertex i, we have

$$E_z^{AD} - E_z^{BC} = E_i - E_{i^k}. \tag{37}$$

For the right-hand side of (30), we have

$$\begin{aligned}&-\jmath\omega\int_l \mathbf{B}_t\cdot\mathbf{a}_n\,dl + M_0\delta(\boldsymbol{\rho}-\boldsymbol{\rho}')\\ &\quad= -\jmath\omega B_{i^k}\int_l \wedge_{i^k}(\boldsymbol{\rho})\cdot\mathbf{a}_n\,dl + M_0\\ &\quad= -\jmath\omega \mathrm{B}_{i^k}\sigma_{i^k}l_{i^k} + M_0\cos\theta\end{aligned} \tag{38}$$

where $\sigma_{i^k} = 1.0$ if $\wedge_{i^k}$ and $\mathbf{a}_n$ are in the same direction and l_{i^k} is the length of the edge i^k. Also, θ is the angle between the normal vector to the edge $\mathbf{a}_n$ and the direction of the current $\mathbf{a}_x$. Thus, using (37) and (38), we can write (30) as

$$E_i - E_{i^k} = -\jmath\omega \mathrm{B}_{i^k}\sigma_{i^k}l_{i^k} + M_0\cos\theta. \tag{39}$$

Using (39) and (36) to eliminate the magnetic field coefficients, we have

$$\sum_{k^i=1}^{K^i}\frac{E_i - E_{i^i}}{-\jmath\omega\sigma_{k^i}l_{k^i}}\nu_{k^i} - \jmath\omega E_i\sum_{j^i=1}^{J^i}\epsilon_{j^i}\frac{A_{j^i}}{3} = \sum_{k^i=1}^{K^i}\frac{M_0\cos\theta\nu_{k^i}}{-\jmath\omega\sigma_{k^i}l_{k^i}} \tag{40}$$

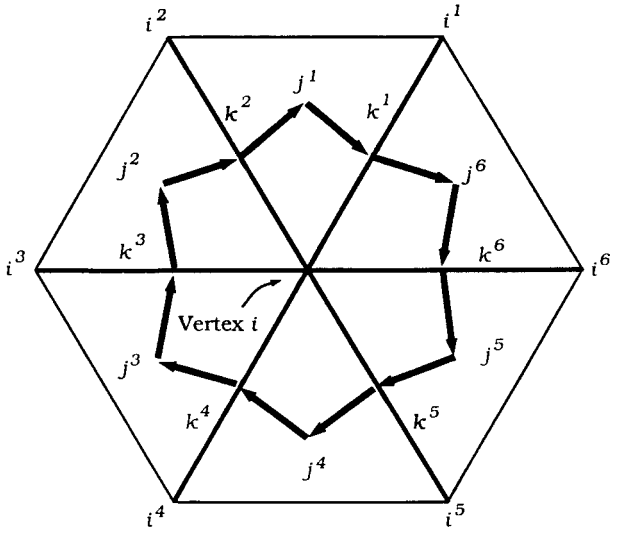

Fig. 9. A vertex i with associated vertices i^i, edges k^i, and triangles j^i. In this case, the local variables $I^i = K^i = J^i = 6$.

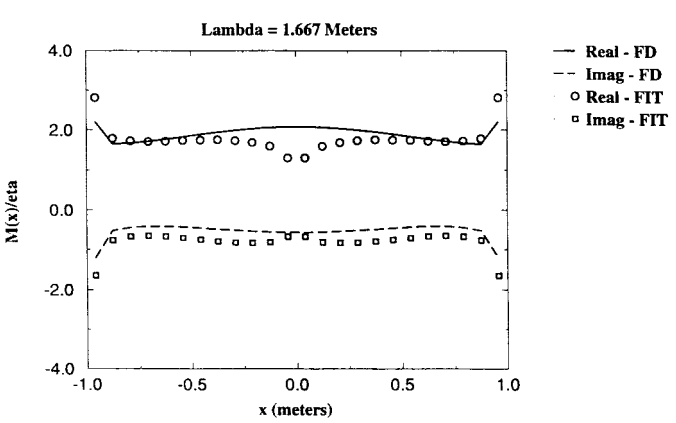

Fig. 10. Equivalent magnetic current on a rectangular cavity-backed slit illuminated by a normal incident TE plane wave.

where now the unknowns are exclusively in terms of the unknown electric field coefficients. By solving (40) for a given excitation, we obtain electric field at each vertex. Next, we use (39) to obtain the magnetic field coefficients. Thus, the elements of Y^C_{pq} are obtained by placing the magnetic current source at x_q, $q = 1, 2, \cdots, N$ and obtaining the corresponding magnetic field at x_p, $p = 1, 2, \cdots, N$. Note that x_p and x_q are located along the slot width.

IV. Numerical Results

In this section, we present the numerical results obtained by the FIT scheme presented in Sections II and III. Although, we have reproduced most of the results presented in [3], [4], for the sake of brevity, we present only rectangular cavity ($1.2\lambda \times 0.8\lambda$) here.

In Figs. 10 and 11, we present the equivalent magnetic current induced on the aperture as function of slot width for normally incident TE and TM plane waves, respectively. The slot region is divided into 24 equal segments. The cavity region is divided into 24 $\times$ 16 squares. By joining the diagonals,

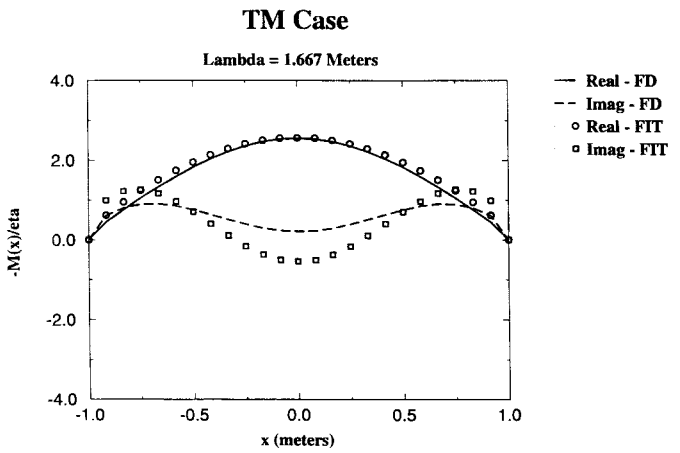

Fig. 11. Equivalent magnetic current on a rectangular cavity-backed slit illuminated by a normal incident TM plane wave.

the region is aproximated by 768 triangular cylinders. For comparison, we also present the finite-difference solution. We note good agreement between both solutions. Further, these results compare well with the FE solutions [3], [4].

V. Conclusion

The purpose of this effort was to validate the FIT method for cavity-backed aperture problems illuminated by TE and TM plane waves. It may be noted that the FIT technique generates a sparse matrix and easily handles inhomogeneous materials and complex geometries. Further, the FIT method is free of spurious solutions. We observed this fact while calculating the modal frequencies of rectangular and circular waveguides. Thus, FIT may be considered as an alternate method to FE solution. Presently, work is in progress to apply the FIT method to three-dimensional problems.

References

[1] S. W. Lee and H. Ling, "Data book for cavity RCS," Tech. Rep. SWL89-1, Electromagnetics Lab., Univ. Illinois, Urbana-Champaign, Jan. 1989.

[2] K. Barkeshli and J. L. Volakis, "Scattering by an aperture formed by a rectangular cavity in a ground plane," Tech. Rep., 389757-1-T, Radiation Lab., Univ. Michigan, Ann Arbor, Dec. 1989.

[3] S. K. Jeng, "Scattering from a cavity-backed slit in a ground plane—TE case," *IEEE Trans. Antennas Propagat.*, vol. 38, pp. 1523–1529, Oct. 1990.

[4] S. K. Jeng and S. T. Tzeng, "Scattering from a cavity-backed slit in a ground plane—TM case," *IEEE Trans. Antennas Propagat.*, vol. 39, pp. 661–663, May 1991.

[5] U. van Rienen and T. Weiland, "Triangular discretization method for the evaluation of rf-fields in cylindrically symmetric cavities," *IEEE Trans. Magn.*, vol. M-21, pp. 2317–2320, Nov. 1985.

[6] J. E. Lebaric and D. Kaijfez, "Analysis of dielectric resonator cavities using the finite integration technique," *IEEE Trans. Microwave Theory Tech.*, vol. 37, pp. 1740–1748, Nov. 1989.

[7] J. E. wheeler III, "Formulation and investigation of finite integral techniques for computing electromagnetic fields in the presence of arbitrary inhomogeneous objects," Ph.D. dissertation, Univ. Houston, Houston, TX, 1991.

[8] R. F. Harrington and J. R. Mautz, "A generalized network for formulation for aperture problems," *IEEE Trans. Antennas Propagat.*, vol. AP-24, pp. 870–873, Nov. 1976.

[9] S. M. Rao, D. R. Wilton, and A. W. Glisson, "Electromagnetic scattering by surfaces of arbitrary shape," *IEEE Trans. Antennas Propagat.*, vol. AP-30, pp. 409–418, May 1982.

Sadasiva M. Rao (M'83–SM'90) received the B.S. degree in electrical communication engineering from Osmania University, the M.S. degree in microwave engineering from Indian Institute of Science, and the Ph.D. degree with a specialization in electromagnetic theory from the University of Mississippi, University, MS, in 1974, 1976, and 1980, respectively.

He served as a Research Assistant at the University of Mississippi and the University of Syracuse, Syracuse, NY, from 1976 to 1980, and as an Assistant Professor in the Department of Electrical Engineering, Rochester Institute of Technology from 1980 to 1985. He was a Senior Scientist at Osmania University from 1985 to 1987. From 1987 to 1988 he was a Visiting Associate Professor in the Department of Electrical Engineering, University of Houston, TX. Currently, he is as a Professor in the Electrical Engineering Department, Auburn University, Auburn, AL. His research interests are in the area of numerical methods applied to antennas and scattering.

Griffin K. Gothard received the B.S., M.S., and Ph.D. degrees, all in electrical engineering, from Auburn University, Auburn, AL, in 1988, 1990, and 1995, respectively.

Since 1995, he has worked as an Electromagnetic Analyst at Harris Corporation, Melbourne, FL. His research interests focus on computational numerical anaylsis techniques applied to electromagnetic interaction problems.

Donald R. Wilton (S'63–M'65–M'70–SM'80–F'87), for photograph and biography, see p. 315 of the March 1997 issue of this TRANSACTIONS.